Broadband indistinguishability from bright parametric downconversion in a semiconductor waveguide

2015 J. Opt. 17 125201

(http://iopscience.iop.org/2040-8986/17/12/125201)

OPEN ACCESS
IOP Publishing
Journal of Optics
J. Opt. 17 (2015) 125201 (9pp)
doi:10.1088/2040-8978/17/12/125201

Broadband indistinguishability from bright parametric downconversion in a semiconductor waveguide

T Günthner[1], B Pressl[1], K Laiho[1], J Geßler[2], S Höfling[2,3], M Kamp[2], C Schneider[2] and G Weihs[1,4]

[1] Institut für Experimentalphysik, Universität Innsbruck, Technikerstraße 25, 6020 Innsbruck, Austria
[2] Technische Physik, Universität Würzburg, Am Hubland, 97074 Würzburg, Germany
[3] School of Physics & Astronomy, University of St Andrews, St Andrews, KY16 9SS, UK
[4] Institute for Quantum Computing, University of Waterloo, 200 University Avenue W, Waterloo, ON, N2L 3G1, Canada

E-mail: thomas.guenthner@uibk.ac.at and kaisa.laiho@uibk.ac.at

Received 30 April 2015, revised 12 August 2015
Accepted for publication 13 August 2015
Published 8 October 2015

Abstract

Parametric downconversion (PDC) in semiconductor Bragg-reflection waveguides (BRW) is routinely exploited for photon-pair generation in the telecommunication range. Contrary to many conventional PDC sources, BRWs offer possibilities to create spectrally broadband but nevertheless indistinguishable photon pairs in orthogonal polarizations that simultaneously incorporate high frequency entanglement. We explore the characteristics of co-propagating twin beams created in a type-II ridge BRW. Our PDC source is bright and efficient, serving as a benchmark of its performance and justifies its exploitation for further use in quantum photonics. We then examine the coalescence of the twin beams and investigate the effect of their inevitable multi-photon contributions on the observed photon bunching. Our results show that BRWs have a great potential for producing broadband indistinguishable photon pairs as well as multi-photon states.

Keywords: parametric downconversion, twin beams, two-photon quantum interference, Bragg-reflection waveguides

1. Introduction

Versatile quantum light sources are needed for a variety of quantum communication tasks, and thus we would like to develop them for the telecommunication wavelengths. Perhaps the best scrutinized process is parametric downconversion (PDC), which produces photons in pairs, usually denoted as signal and idler. Waveguide realizations have turned PDC sources into easy-to-handle and small-scale tools that moreover provide higher brightness than their bulk counterparts [1, 2]. Waveguided sources further provide better integrability and quantum integrated networks have been built both on semiconductor as well as ferro- and dielectric platforms [3–6].

Recently, we and others demonstrated PDC in waveguides being composed of layers of semiconductor materials that are historically named Bragg-reflection waveguides (BRWs) [7–9]. In comparison to ferroelectric non-linear optical waveguides the semiconductor structures benefit from higher nonlinearity and better integrability [9]. By embedding the pump laser and the photon-pair production on the same chip the PDC emission can even be electrically self-pumped [10, 11]. BRWs with high signal-idler correlations are suitable for various quantum optical tasks [9, 12]. Previous experimental studies include the investigation of the photon-pair indistinguishability [13] and preparation of polarization entangled states both with co- and counter-propagating signal

and idler schemes [14–16]. Furthermore, BRWs offer a lot of flexibility for source design, which aims at engineering of quantum states with desired properties for specific applications [17–22].

However, in order to successfully compete with conventional PDC sources, BRWs have to be able to produce twin beams, in other words signal and idler obeying a strict photon-number correlation, in a bright and efficient manner with a low number of spurious counts [8, 9]. Still today, their drawbacks are the incompatibility of the utilized spatial modes with standard single-mode fiber optics, a rather high facet reflectivity because of the large refractive index difference with air, and a high numerical aperture (NA) due to the strong confinement of the spatial modes. On top of this, the optical losses both at the pump and the downconverted wavelengths are significant [9, 23], which limits the useful length of the structures.

The phasematching required for the PDC process can be achieved in semiconductor waveguides by spatial mode matching [24–26] eliminating the need for quasi-phase-matching, which is typical for conventional sources. All in all, the characteristics of signal and idler in their different degrees of freedom are determined by the PDC process parameters such as the strength of the nonlinearity, pump envelope and the dispersion of the interacting modes in the used geometry. The resulting joint spectrum of signal and idler to a large extent dictates for which quantum optics applications the photonic source in question is suitable [27–29]. The state-of-the-art BRW sources provide high entanglement in the spectral degree of freedom [30–32]. Simultaneously, they also offer broadband spectral indistinguishability for signal and idler that are created in orthogonal polarizations. The former is desired in applications requiring multimode PDC characteristics—or higher dimensional states [33, 34], whereas the latter is a building block for many quantum optical networks that usually base on photon interference [35–37]. The PDC process parameters also govern the photon statistics of the twin beams, inevitably resulting in higher photon-number contributions, which have to be controlled [38].

Here, we investigate the characteristics of spectrally broadband type-II PDC emitted by a BRW in a single-pass configuration. First, we determine the Klyshko efficiency of our BRW source. Thereafter, we utilize correlation functions between signal and idler in order to investigate the mean photon number in them. We further test the broadband indistinguishability in a two-photon coalescence experiment. For this purpose, we manipulate the spectral bandwidth of signal and idler by broadband filtering, and via their bunching at different gains we determine the indistinguishability governed by the spectral overlap. Our results show that BRWs are bright and efficient photon sources.

2. Sample design and experiment

Our BRW sample depicted schematically in figure 1(a) is grown on a GaAs substrate by molecular beam epitaxy. The sample, having the same structural design as in [9, 15], is made of $Al_x\ Ga_{1-x}As$ $(0 < x < 1)$ compounds because of their inherent high optical second order nonlinearity and the sophisticated fabrication techniques available. Due to its zincblende structure, $Al_x\ Ga_{1-x}As$ has no birefringence and, therefore, in order to achieve phasematching the sample is designed to support different spatial modes that are the Bragg mode for the pump and the total internal reflection (TIR) modes for the twin beams [40]. The distributed Bragg reflectors (DBRs) embed a multi-layer core that guarantees good spatial overlap of the pump, signal and idler mode triplets required for an efficient PDC process [41–43]. Finally, the ridge structure is fabricated by electron beam lithography followed by plasma etching. This ensures mode confinement in two dimensions—in the vertical direction by the DBRs and in the horizontal direction by the ridge structure.

In our experiment as shown in figure 1(b) we employ a picosecond pulsed Ti:Sapphire laser (76.2 MHz repetition rate, 772 nm central wavelength) as a pump for the PDC process. After power, polarization and spatial mode control, we focus the pump on to the front facet of our BRW with a 100x microscope objective (MO), which allows reasonably efficient coupling into the Bragg mode. At its output facet a high NA aspheric lens (AL) collects the PDC emission from our BRW, for which we numerically determined the NAs of approximately 0.2 and 0.5 in the horizontal and vertical direction, respectively [39]. After removing the residual pump beam with a dichroic mirror (DM), we use a band-pass filter (BPF) with either a 12 nm or 40 nm bandwidth to spectrally limit the twin beams. With an additional half-wave plate (HWP) we change the polarization direction of signal and idler, as necessary for the coalescence experiment. After separating the orthogonal polarizations using a polarizing beam splitter (PBS), we launch each beam to a single-mode fiber for detection with two commercial time-gated InGaAs avalanche photo-diodes (APDs). By utilizing a narrowband telecom laser for adjustment, we estimate that the TIR modes can be coupled with up to 50% efficiency into the used fibers, excluding other optical losses on the beam path. Additionally, the variable photodetection probability of our APDs is set either to 20% or 25% resulting in dark count rates of about 70 $s^{-1}$and 200 s^{-1}, correspondingly. Finally, we employ a time to digital converter to discriminate the single and coincidence counts. Due to technical limitations, only every 64th laser pulse gates our InGaAs APDs corresponding to a rate R of about 1.19 MHz.

3. Source efficiency and brightness

With conventional PDC sources efficient single-mode fiber couplings and large mean photon numbers can be achieved at telecommunication wavelengths [34, 44–46]. Therefore, we start by investigating the performance of our BRW source by determining its Klyshko efficiency [47] and thereafter evaluate the mean photon number in the individual twin beams. For this purpose we use the configuration shown in figure 1(b), in which the PDC emission is filtered to a spectral width of 40 nm to suppress background light from the waveguide before the signal and idler beams are deterministically separated at the PBS.

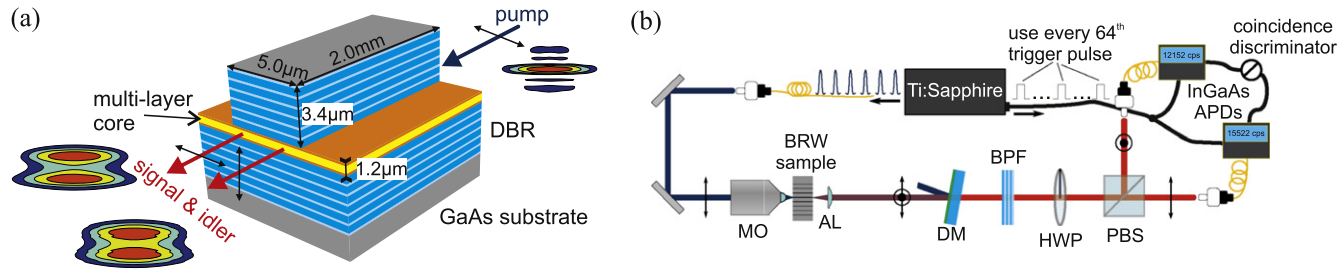

Figure 1. (a) Investigated BRW sample with a core thickness of 1.2 μm, a length of 2.0 mm and a ridge width and height of 5.0 μm and 3.4 μm, respectively. The depicted amplitude distributions of pump, signal and idler mode were inferred with a commercial-grade simulator eigenmode solver and propagator [39]. (b) Experimental setup for investigating the source efficiency and brightness as well as the signal and idler coalescence. For abbreviations and more details see text.

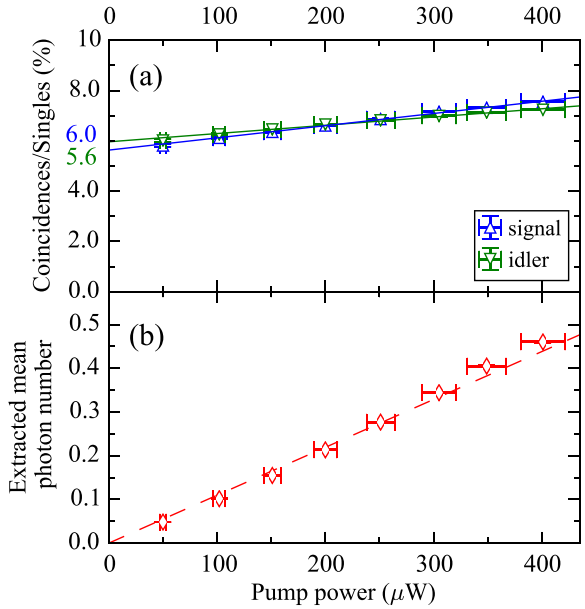

Figure 2. (a) The ratio of coincidences to singles in both signal and idler and (b) mean photon number $\langle n \rangle$ in one of the generated twin beams with respect to the pump power. The vertical errorbars are smaller than the used symbols.

To eliminate the effect of the accidental coincidences produced by the higher photon-number contributions created in PDC, we measure the process efficiency with respect to the pump power. In the region of weak pump powers we can extract the Klyshko efficiency, which is defined only for perfectly photon-number correlated photon-pairs, as $\eta_{s,i} = C/S_{i,s}$ with C being the coincidence rate and $S_{s,i}$ the single count rates of signal and idler, respectively. Our results in figure 2(a) show the ratio of coincidence counts to single counts for both signal and idler detected with a chosen nominal photon detection probability of 20% of our APDs. Thence, we extrapolate Klyshko efficiencies of 6.0(1)% and 5.6(2)% for signal and idler, respectively. This indicates that despite the high NA and the complex spatial mode structure, the PDC emission can be fairly efficiently collected with standard single-mode optics even when compared with the performance of the conventional sources [45, 46].

By extracting the signal and idler cross-correlation C/A, in which $A = S_i S_s/R$ corresponds to the accidental count rate, we can further estimate the mean photon number $\langle n \rangle$ created in one of the twin beams in a loss-independent manner via $C/A \approx 1/\langle n \rangle + 1$ [48]. Since our BRW is a highly multimodal PDC source (see appendix A), this estimate gives the mean photon number in good approximation, being in the worst case the lower bound. In figure 2(b) we illustrate the obtained mean photon number growing linearly with respect to the increasing pump power as expected for weakly excited PDC. Our results show that mean photon numbers up to 0.5 can be achieved with moderate pump powers. This further indicates that the PDC multi-photon contributions have to be taken into account especially in the photon coalescence experiment we investigate next.

4. Coalescence of signal and idler

For observing the coalescence of signal and idler photons we follow the experiment in [31] and investigate photon bunching by varying their distinguishability in the polarization degree of freedom. For this purpose, we detect the coincidences between signal and idler while rotating the HWP in figure 1(b). In case the HWP axes are oriented parallel to the cross-polarized signal and idler, they are separated deterministically at the PBS. In any other case, signal and idler bunch together if they are indistinguishable in all degrees of freedom—not only in polarization but also spatially and spectrally.

We record the coincidence counts with respect to the HWP angle at several pump powers. Additionally, we change the photon detection probability of our APDs from 20% to 25% to increase the count rates. Figures 3(a) and (b) show our results with a 12 nm BPF for a low and a high pump power value, respectively. From this, we can directly conclude that the higher the pump power the lower is the visibility of the measured fringes given by $\mathcal{V} = (C_{\max.} - C_{\min.})/(C_{\max.} + C_{\min.})$. We nevertheless achieved a maximum visibility of 0.83(1), which lies significantly above the classical limit of 1/3 for a completely distinguishable photon pair with no higher-order contributions [31] and delivers a measure of the signal and idler indistinguishability.

In order to understand the effect of the multi-photon contributions to the signal and idler coalescence, we further

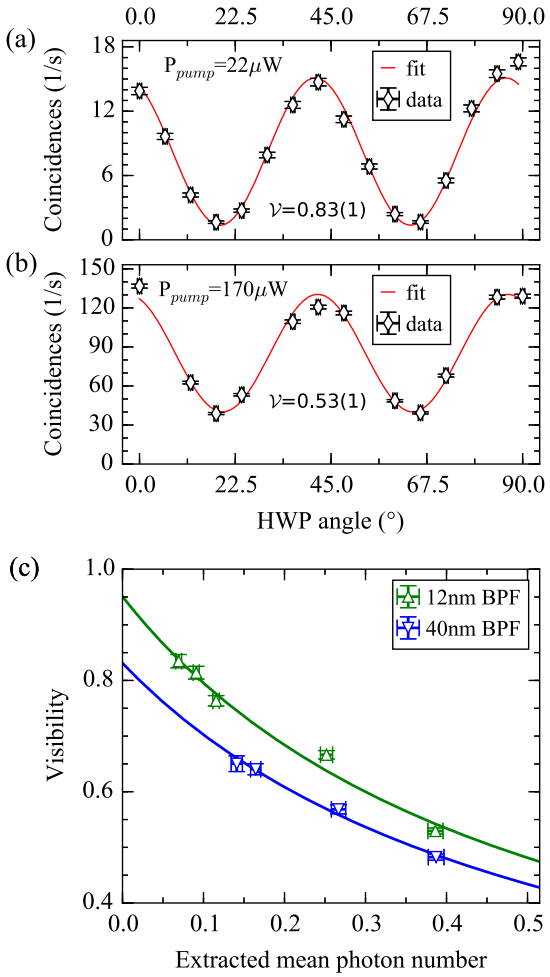

Figure 3. Measured coincidence counts as function of the HWP angle for pump powers of (a) 22 μW and (b) 170 μW for a 12 nm filter bandwidth. (c) The extracted visibilities decrease with increasing mean photon number.

examine the visibility in terms of the mean photon number, which is also directly provided by the measured data, when signal and idler are deterministically split at the PBS. In figure 3(c) we depict the measured visibilities with respect to the estimated mean photon numbers for both 12 nm and 40 nm BPFs. In both cases the visibility clearly decreases with increasing mean photon number. However, not only the increasing multi-photon contributions but also the spectral mismatch between signal and idler affect the visibility in the coalescence experiment. From the measured visibilities we can infer the spectral overlap of the downconverted photon pairs via (see appendix B)

$$\mathcal{V} \approx \frac{1+\mathcal{O}}{3-\mathcal{O}+4\langle n\rangle}. \tag{1}$$

By fitting our results in figure 3(c) against (1) we retrieve for the spectral overlap with 12 nm and 40 nm filter bandwidths the values of 95.0(6)% and 81.6(9)%, respectively. The large difference in the spectral overlaps with the two investigated filters are caused by the fact that signal and idler wavepackets are temporally shifted with respect to each other due to their slightly different group velocities. Theoretically, the *joint spectral distribution* of signal and idler governs the spectral overlap (see appendix A). Our results are in good accordance with numerical simulations, which predict spectral overlaps of about 98% and 83%, respectively, for the two filters.

5. Conclusion

Integratable and easy-to-handle sources of parametric down-conversion are highly desired in many quantum optics applications. Bragg-reflection waveguides based on semi-conductor compounds provide a platform that can meet these demands. Our BRW sample shows a good performance, and we can reach Klyshko efficiencies up to a few percent with avalanche photodetection, regardless of the non-standard mode profile of the signal and idler beams. Moreover, our source provides a high brightness and is capable of producing higher photon numbers as is desired for multiphoton production. We further examined the coalescence between the twin beams filtered to a few tens of nanometers bandwidth in order to assess their indistinguishability. The visibility of the measured fringes is diminished by the multi-photon contributions of signal and idler, but we can nevertheless extract a high degree of indistinguishability, which is quantified by their spectral overlap. We extended our model to take into account both these process parameters and showed that our results are in good agreement with numerical simulations. Thus, being characteristic for BRWs, our source provides signal and idler in orthogonal polarizations that are over a broad spectral band highly indistinguishable in frequency. We believe our work gives a detailed insight of the PDC process in our BRW both in the spectral and photon-number degrees of freedom. This will become important when optimizing and adapting BRW sources into quantum optical networks.

Acknowledgments

We thank Matthias Covi for assistance with the experimental setup. This work was supported in part by the ERC, project *EnSeNa* (257531) and by the FWF through project no. I-2065-N27.

Appendix A. Modelling the joint spectral properties of signal and idler

In this appendix we investigate the joint spectral amplitude (JSA) of signal and idler and numerically estimate the spectral overlap $\mathcal{O}$, which determines their indistinguishability in the low gain regime. Following [27, 28, 49] we find that the joint spectral characteristics in a collinear single-pass PDC source are given by

$$f(\omega_s, \omega_i) = \frac{1}{\mathcal{N}}\alpha(\omega_s+\omega_i)\phi(\omega_s, \omega_i), \tag{A.1}$$

in which $\mathcal{N}$ accounts for the normalization of the JSA via $\int \mathrm{d}\omega_s \mathrm{d}\omega_i |f(\omega_s, \omega_i)|^2 = 1$, $\alpha(\omega_p = \omega_s + \omega_i)$ describes the

Table A1. Parameters of the pump (p), signal (s) and idler (i) mode extracted from numerical simulations [39].

$v_{g(\mu)}$ (μm/ps)			κ_μ ($\cdot 10^{-3}$ ps/μm)		Λ_μ ($\cdot 10^{-6}$ ps^2/μm)		
p	s	i	s	i	p	s	i
74.0	90.1	90.4	−2.40	−2.44	5.74	−2.16	−2.17

pump spectrum in terms of the frequencies ω_μ ($\mu = p, s, i$) for pump, signal and idler, respectively, and $\phi(\omega_s, \omega_i)$ is the phasematching (PM) function. In a Gaussian approximation we can describe the pump amplitude as

$$\alpha(\omega_s + \omega_i) = \mathrm{e}^{-\frac{1}{\sigma_p^2}(\omega_s+\omega_i)^2} \tag{A.2}$$

with σ_p being the bandwidth of the pump. We use a simple PDC model for uniform waveguides [29, 42] with constant-valued non-linearity over the whole length of the waveguide and assume that the overlap of spatial modes effectively affects only its strength. Thus, in the single-pass configuration we can write the PM function as [50]

$$\begin{aligned}\phi(\omega_s, \omega_i) &= \mathrm{sinc}\left(\frac{L}{2}\Delta k(\omega_s, \omega_i)\right)\mathrm{e}^{\mathrm{i}\frac{L}{2}\Delta k(\omega_s,\omega_i)} \\ &\approx \mathrm{e}^{-\gamma\frac{L^2}{4}\Delta k^2(\omega_s,\omega_i)}\mathrm{e}^{\mathrm{i}\frac{L}{2}\Delta k(\omega_s,\omega_i)},\end{aligned} \tag{A.3}$$

in the final form of which we have used a Gaussian approximation for the sinc-function. In (A.3) L denotes the BRW length, $\Delta k(\omega_s, \omega_i) = k_p(\omega_s + \omega_i) - k_s(\omega_s) - k_i(\omega_i)$ describes the phase mismatch in terms of $k_\mu(\omega_\mu) = n_\mu\omega_\mu/c$ with n_μ being the effective refractive index and c the speed of light, while $\gamma \approx 0.193$ adjusts the width of the approximated PM function. Performing a Taylor expansion of Δk to the second order at a phasematched point $\omega_p^0 = \omega_s^0 + \omega_i^0$ we can write the phase mismatch as

$$\Delta k(\omega_s, \omega_i) \approx \kappa_s\nu_s + \kappa_i\nu_i + \Lambda_s\nu_s^2 + \Lambda_i\nu_i^2 - \Lambda_p\nu_s\nu_i, \tag{A.4}$$

in which the detunings are defined as $\nu_\mu = \omega_\mu - \omega_\mu^0$. In (A.4) $\kappa_\mu = k'_\mu(\omega_\mu^0) - k'_p(\omega_p^0) = 1/v_{g(\mu)} - 1/v_{g(p)}$ is determined by the group velocity mismatch of the downconverted photons and the pump photon, while $\Lambda_{s,i} = \frac{1}{2}k''_{s,i}(\omega_{s,i}^0) - \frac{1}{2}k''_p(\omega_p^0)$ and $\Lambda_p = k''_p(\omega_p^0)$ are related to the group velocity dispersions.

For our simulation we substitute (A.2)–(A.4) into (A.1) and evaluate the JSA. From a commercially available solver (Mode Solutions [39]) we obtain for the PDC process in our BRW (in figure 1(a)) the dispersion properties listed in table A1. In figure A1 we show the joint spectral intensity (JSI), $|f(\omega_s, \omega_i)|^2$, as a function of the signal and idler frequencies $f_{s,i} = \omega_{s,i}/2\pi$. We evaluated JSI at the extracted degeneracy point of $f_s^0 = f_i^0 = 193.3$ THz corresponding to 1551.1 nm with a pump having a 0.25 nm broad spectrum. The simulated degeneracy point is very close to the measured one found at 1544.1(8) nm. We believe this slight discrepancy is due to the experimental limitations in the BRW growth process concerning the accuracy at which the refractive index and the thickness of the layers can be controlled.

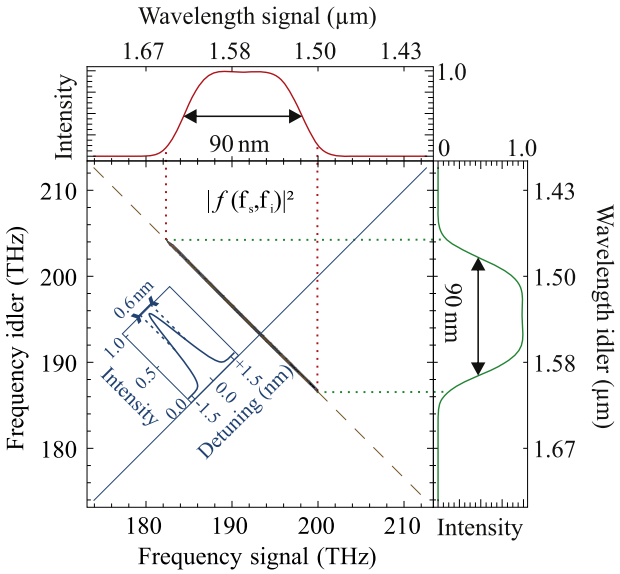

Figure A1. A contour plot of JSI with respect to the signal and idler frequencies/wavelengths. The inset illustrates the width of the JSI in terms of detuning from the degeneracy point. The red and green solid curve represent the marginal spectra. The diagonal (blue solid line) and the anti-diagonal (brown dashed line) as well as the dotted lines provide guides for the eye.

Due to small difference in the group velocities of the signal and idler photons in the vicinity of the degeneracy point, the tilt of the PM function $\theta \approx \arctan(\kappa_s/\kappa_i)$ deviates from that of perfect anti-correlation by about 0.5°. Altogether, our simulated JSI is slightly asymmetric around the degeneracy point, leading to different spectral properties of signal and idler centered at 1567 nm and 1535 nm, respectively. Both marginal spectra are originally approximately 90 nm wide. Thus, they are two orders of magnitude broader than the linewidth of the JSI at its degeneracy point, being about 0.6 nm as shown in the inset in figure A1. Therefore, even in the case of spectral filtering we expect a highly multimodal PDC emission [32] from our BRW sample and almost perfectly spectrally indistiguishable twin beams.

The spectral overlap is determined by [31] $\mathcal{O} = \int\int \mathrm{d}\omega_s \mathrm{d}\omega_i\, f(\omega_s, \omega_i) f^*(\omega_i, \omega_s)$ and depends remarkably on the group velocity mismatch. As in our case signal and idler travel with slightly different group velocities, their wavepackets are temporally shifted, which is evident from the phase term of the JSA. For the unfiltered JSA we determine a spectral overlap of only about 26%, while 76% could be achieved if the temporal mismatch was corrected. We restrict the influence of the group velocity mismatch by spectral filtering close to the JSA degeneracy point and, therefore, we

expect a spectral overlap of about 98% and 83% when filtering with a 12 nm (1.5 THz) Gaussian and a 40 nm (5.0 THz) super-Gaussian BPF, respectively. These values are in good accordance with our experimentally determined results in section 4.

Appendix B. Quantum interference experiment with a twin beam state

We utilize the description of parametric downconversion as multimode squeezer in order to estimate the effect of the higher photon-number contributions on a quantum interference between signal and idler [48, 51]. We start by considering the configuration in figure B1, in which the bunching takes place at a symmetric beam splitter having a transmission of $T = 1/2$ corresponding to the case of recording the minimum amount of coincidences in our coalescence measurement. Prior that signal and idler are subjected to losses as is the case also in our experimental realization.

We define the transformation between the system input arms, a and b, and output arms, c and d, in time t as

$$\hat{\mathbf{c}}(t_1) = 1/\sqrt{2}\Big[\sqrt{\eta_1}\,\hat{\mathbf{a}}(t_1) + \sqrt{1-\eta_1}\,\hat{\mathbf{v}}_1(t_1) + \sqrt{\eta_2}\,\hat{\mathbf{b}}(t_1) + \sqrt{1-\eta_2}\,\hat{\mathbf{v}}_2(t_1)\Big] \tag{B.1}$$

$$\hat{\mathbf{d}}(t_2) = 1/\sqrt{2}\Big[\sqrt{\eta_1}\,\hat{\mathbf{a}}(t_2) + \sqrt{1-\eta_1}\,\hat{\mathbf{v}}_1(t_2) - \sqrt{\eta_2}\,\hat{\mathbf{b}}(t_2) - \sqrt{1-\eta_2}\,\hat{\mathbf{v}}_2(t_2)\Big], \tag{B.2}$$

which expresses the photon annihilators $\hat{\mathbf{c}}(t_\varsigma)$ and $\hat{\mathbf{d}}(t_\varsigma)$ ($\varsigma = 1, 2$) at the beam splitter output ports in terms of those of the inputs $\hat{\mathbf{a}}(t_\varsigma)$ and $\hat{\mathbf{b}}(t_\varsigma)$ and the vacuum modes $\hat{\mathbf{v}}_{1,2}(t_\varsigma)$. The detection efficiencies correspond to the transmission coefficients $\eta_{1,2}$. Further, we assume that our detectors have a spectrally broad response and their detection windows are much longer than the duration of the generated pulsed wavepackets. Thus, the coincidence rate can be evaluated via [27]

$$\mathcal{R} \propto \int \mathrm{d}t_1 \int \mathrm{d}t_2 \left\langle \hat{\mathbf{c}}^\dagger(t_1)\hat{\mathbf{d}}^\dagger(t_2)\hat{\mathbf{d}}(t_2)\hat{\mathbf{c}}(t_1)\right\rangle, \tag{B.3}$$

the integrand in which describes the probability of a coincidence at times t_1 and t_2 between the two detectors.

Our goal is to rewrite (B.3) in terms of the beam splitter input operators and then evaluate the expectation values regarding the desired input state. By plugging the beam splitter transformations in (B.1) and (B.2) together with their conjugates to (B.3) and utilizing the Fourier transformations given by $\hat{\mathbf{a}}(t) = \frac{1}{\sqrt{2\pi}}\int \mathrm{d}\omega\ \hat{\mathbf{a}}(\omega)\mathrm{e}^{-\mathrm{i}\omega t}$ and $\hat{\mathbf{b}}(t) = \frac{1}{\sqrt{2\pi}}\int \mathrm{d}\omega\ \hat{\mathbf{b}}(\omega)\mathrm{e}^{-\mathrm{i}\omega t}$ with ω being the optical angular frequency, only few terms survive and we can write down the

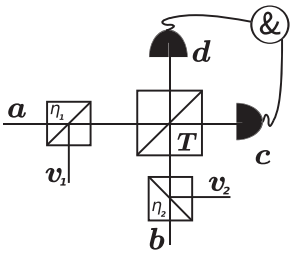

Figure B1. Model of bunching experiment with a twin beam state. The twin beams send to the input arms a and b are degraded due to losses at the beam splitters with transmissions η_1 and η_2, to which the optical vacuum modes v_1 and v_2 are coupled, respectively. Bunching occurs at the beam splitter with transmission T and coincidences are counted between the two output arms c and d. For more details see text.

coincidence rate in the form

$$\begin{aligned}\mathcal{R} \propto \frac{1}{4}\Big\langle \int \mathrm{d}\omega \int \mathrm{d}\tilde{\omega}\ \Big[&\eta_1^2\hat{\mathbf{a}}^\dagger(\omega)\hat{\mathbf{a}}^\dagger(\tilde{\omega})\hat{\mathbf{a}}(\tilde{\omega})\hat{\mathbf{a}}(\omega)\\ &- \eta_1\eta_2\hat{\mathbf{a}}^\dagger(\omega)\hat{\mathbf{a}}^\dagger(\tilde{\omega})\hat{\mathbf{b}}(\tilde{\omega})\hat{\mathbf{b}}(\omega)\\ &- 2\eta_1\eta_2\hat{\mathbf{a}}^\dagger(\omega)\hat{\mathbf{b}}^\dagger(\tilde{\omega})\hat{\mathbf{a}}(\tilde{\omega})\hat{\mathbf{b}}(\omega)\\ &+ 2\eta_1\eta_2\hat{\mathbf{a}}^\dagger(\omega)\hat{\mathbf{b}}^\dagger(\tilde{\omega})\hat{\mathbf{b}}(\tilde{\omega})\hat{\mathbf{a}}(\omega)\\ &- \eta_1\eta_2\hat{\mathbf{b}}^\dagger(\omega)\hat{\mathbf{b}}^\dagger(\tilde{\omega})\hat{\mathbf{a}}(\tilde{\omega})\hat{\mathbf{a}}(\omega)\\ &+ \eta_2^2\hat{\mathbf{b}}^\dagger(\omega)\hat{\mathbf{b}}^\dagger(\tilde{\omega})\hat{\mathbf{b}}(\tilde{\omega})\hat{\mathbf{b}}(\omega)\Big]\Big\rangle,\end{aligned} \tag{B.4}$$

in which we have carried out the integration over time by extending the limits to infinity $\left(\delta(\omega) = 1/(2\pi)\int_{-\infty}^{\infty}\mathrm{d}t_\mu \mathrm{e}^{\mathrm{i}t_\mu\omega}\right)$.

Now, we re-express (B.4) in terms of broadband detection modes that correspond to those of our downconverter. The multimode squeezed state sent to the input arms a and b of the beam splitter is defined via the unitary squeezing operator $\hat{\mathbf{S}}_{a,b}$ as [48]

$$\langle\Psi\rangle = \hat{\mathbf{S}}_{a,b}\langle 0\rangle = \mathrm{e}^{\sum_k r_k\hat{\mathbf{A}}_k^\dagger\hat{\mathbf{B}}_k^\dagger - h.c.}\langle 0\rangle, \tag{B.5}$$

in which the real valued squeezing strength $r_k = \mathcal{B}\lambda_k$ is related to the gain of the PDC process $\mathcal{B}$ and to the Schmidt modes λ_k ($\sum_k \lambda_k^2 = 1$) of the joint spectral correlation function of signal and idler given by $f(\omega_s, \omega_i) = \sum_k \lambda_k \varphi_k(\omega_s)\phi_k(\omega_i)$. With the help of the two sets of orthonormal basis functions $\{\varphi_k\}$ and $\{\phi_k\}$ for signal and idler, respectively, we define the k-th mode sent to the input arm a as

$$\hat{\mathbf{A}}_k^\dagger = \int \mathrm{d}\omega\ \varphi_k(\omega)\ \hat{\mathbf{a}}^\dagger(\omega), \tag{B.6}$$

for which the following relations hold:

$$\int \mathrm{d}\omega\ \varphi_k^*(\omega)\varphi_{k'}(\omega) = \begin{cases}1 & \text{if } k = k',\\ 0 & \text{otherwise}\end{cases} \quad \text{and}$$
$$\sum_k \varphi_k(\omega)\varphi_k^*(\tilde{\omega}) = \delta(\omega - \tilde{\omega}). \tag{B.7}$$

Similarly, the k-th mode sent to the input arm b can be written as

$$\hat{\mathbf{B}}_k^\dagger = \int \mathrm{d}\omega\ \phi_k(\omega)\ \hat{\mathbf{b}}^\dagger(\omega), \tag{B.8}$$

the basis functions in which obey conditions similar to those in (B.7). The broadband mode transformations of the k-th input modes can be presented in the form [48]

$$\hat{\mathbf{S}}_{a,b}^\dagger \hat{\mathbf{A}}_k \hat{\mathbf{S}}_{a,b} = \cosh(r_k)\hat{\mathbf{A}}_k + \sinh(r_k)\hat{\mathbf{B}}_k^\dagger \tag{B.9}$$

$$\hat{\mathbf{S}}_{a,b}^\dagger \hat{\mathbf{B}}_k \hat{\mathbf{S}}_{a,b} = \cosh(r_k)\hat{\mathbf{B}}_k + \sinh(r_k)\hat{\mathbf{A}}_k^\dagger. \tag{B.10}$$

In the following we consider only the case of weak squeezing and approximate $\sinh(r_k) \approx r_k = \mathcal{B}\lambda_k$ and $\cosh(r_k) \approx 1$. Further, we estimate the mean photon number in the both input arms as $\langle n\rangle = \sum_k \sinh^2(r_k) \approx \mathcal{B}^2$.

In order to transform (B.4) to the broadband-mode picture, we require the identities

$$\begin{aligned}\hat{\mathbf{a}}^\dagger(\omega) &= \sum_k \hat{\mathbf{A}}_k^\dagger \varphi_k^*(\omega) \quad \text{and}\\ \hat{\mathbf{b}}^\dagger(\omega) &= \sum_k \hat{\mathbf{B}}_k^\dagger \phi_k^*(\omega).\end{aligned} \tag{B.11}$$

Thence, we re-express the coincidence rate in (B.4) as

$$\begin{aligned}\mathcal{R} \propto \frac{1}{4}\Bigg\langle \Bigg[& \eta_1^2 \sum_{k,n} \hat{\mathbf{A}}_n^\dagger \hat{\mathbf{A}}_k^\dagger \hat{\mathbf{A}}_k \hat{\mathbf{A}}_n \\ & - \eta_1\eta_2 \sum_{k,n,l,m} \hat{\mathbf{A}}_n^\dagger \hat{\mathbf{A}}_k^\dagger \hat{\mathbf{B}}_l \hat{\mathbf{B}}_m \int \mathrm{d}\omega \varphi_n^*(\omega)\phi_m(\omega) \\ & \times \int \mathrm{d}\tilde{\omega} \varphi_k^*(\tilde{\omega})\phi_l(\tilde{\omega}) \\ & - 2\eta_1\eta_2 \sum_{k,n,l,m} \hat{\mathbf{A}}_n^\dagger \hat{\mathbf{B}}_k^\dagger \hat{\mathbf{A}}_l \hat{\mathbf{B}}_m \int \mathrm{d}\omega \varphi_n^*(\omega)\phi_m(\omega) \\ & \times \int \mathrm{d}\tilde{\omega} \phi_k^*(\tilde{\omega})\varphi_l(\tilde{\omega}) \\ & + 2\eta_1\eta_2 \sum_{k,n} \hat{\mathbf{A}}_n^\dagger \hat{\mathbf{B}}_k^\dagger \hat{\mathbf{B}}_k \hat{\mathbf{A}}_n \\ & - \eta_1\eta_2 \sum_{k,n,l,m} \hat{\mathbf{B}}_n^\dagger \hat{\mathbf{B}}_k^\dagger \hat{\mathbf{A}}_k \hat{\mathbf{A}}_n \int \mathrm{d}\omega \phi_n^*(\omega)\varphi_m(\omega) \\ & \times \int \mathrm{d}\tilde{\omega} \phi_k^*(\tilde{\omega})\varphi_l(\tilde{\omega}) \\ & + \eta_2^2 \sum_{k,n} \hat{\mathbf{B}}_n^\dagger \hat{\mathbf{B}}_k^\dagger \hat{\mathbf{B}}_k \hat{\mathbf{B}}_n \Bigg]\Bigg\rangle.\end{aligned} \tag{B.12}$$

We directly recognize that several terms in (B.12) correspond to Glauber correlation functions $\mathcal{G}(w, v) = \left\langle :\left(\sum_q \hat{\mathbf{A}}_q^\dagger \hat{\mathbf{A}}_q\right)^w \left(\sum_{q'} \hat{\mathbf{B}}_{q'}^\dagger \hat{\mathbf{B}}_{q'}\right)^v : \right\rangle$ with indices w and v describing the order of the correlation for the twin beam modes a and b, respectively [48]. Thence, when disregarding the losses, the expectation values in the first and last terms deliver $\mathcal{G}(2, 0) = \mathcal{G}(0, 2) = \langle n\rangle^2[1 + \frac{1}{K}]$, and in the fourth term $\mathcal{G}(1, 1) = \langle n\rangle^2[1 + \frac{1}{K}] + \langle n\rangle$, where K corresponds to the effective number of excited modes ($K = 1/\sum_k \lambda_k^4$) [48].

The rest of the mean values can be evaluated by plugging in the transformations from (B.9) and (B.10) together with their hermitian conjugates. While the second and fifth terms vanish, the third term delivers

$$\begin{aligned}&\left\langle \sum_{k,n,l,m} \hat{\mathbf{A}}_n^\dagger \hat{\mathbf{B}}_k^\dagger \hat{\mathbf{A}}_l \hat{\mathbf{B}}_m \int \mathrm{d}\omega \varphi_n^*(\omega)\phi_m(\omega) \int \mathrm{d}\tilde{\omega} \phi_k^*(\tilde{\omega})\varphi_l(\tilde{\omega}) \right\rangle \\ &\quad = \langle n\rangle \mathcal{O} + \langle n\rangle^2 \mathcal{A},\end{aligned} \tag{B.13}$$

in which

$$\begin{aligned}\mathcal{O} &= \int \mathrm{d}\omega \int \mathrm{d}\tilde{\omega}\ f^*(\omega, \tilde{\omega}) f(\tilde{\omega}, \omega) \\ &= \sum_{k,n} \lambda_n \lambda_k \int \mathrm{d}\omega \varphi_n^*(\omega)\phi_k(\omega) \int \mathrm{d}\tilde{\omega} \phi_n^*(\tilde{\omega})\varphi_k(\tilde{\omega})\end{aligned} \tag{B.14}$$

describes the spectral overlap between signal and idler and

$$\begin{aligned}\mathcal{A} &= \int \mathrm{d}\omega \int \mathrm{d}\tilde{\omega}\ g_s(\omega, \tilde{\omega}) g_i(\tilde{\omega}, \omega) \\ &= \sum_{k,n} \lambda_n^2 \lambda_k^2 \int \mathrm{d}\omega \varphi_n^*(\omega)\phi_k(\omega) \int \mathrm{d}\tilde{\omega} \phi_k^*(\tilde{\omega})\varphi_n(\tilde{\omega})\end{aligned} \tag{B.15}$$

determines the overlap of signal and idler spectral densities that are given by

$$g_s(\omega, \tilde{\omega}) = \int \mathrm{d}\omega_i\ f^*(\omega, \omega_i) f(\tilde{\omega}, \omega_i) \quad \text{and} \tag{B.16}$$

$$g_i(\tilde{\omega}, \omega) = \int \mathrm{d}\omega_s\ f^*(\omega_s, \tilde{\omega}) f(\omega_s, \omega). \tag{B.17}$$

We note that if the spectral densities of signal and idler are equal this term will end up giving the purity of the photon wavepacket $1/K$.

Finally, we determine an expression for the visibility of our quantum interference experiment in section 4. When signal and idler are expected to bunch, we can estimate the rate of the coincidences according to (B.12) as

$$\begin{aligned}\mathcal{R}_{\min.} \propto & \frac{1}{4}\langle n\rangle^2 \left(1 + \frac{1}{K}\right)\left(\eta_1^2 + \eta_2^2\right) \\ & + \frac{1}{2}\left(\langle n\rangle + \langle n\rangle^2\left(1 + \frac{1}{K}\right)\right)\eta_1\eta_2 \\ & - \frac{1}{2}\left(\langle n\rangle \mathcal{O} + \langle n\rangle^2 \mathcal{A}\right)\eta_1\eta_2.\end{aligned} \tag{B.18}$$

This rate is compared with the one obtained when the signal and idler beams are separated deterministically. By using the same model as above but assuming a beam splitter with $T = 1$ in figure B1, we gain

$$\mathcal{R}_{\max.} \propto \left(\langle n\rangle + \langle n\rangle^2\left(1 + \frac{1}{K}\right)\right)\eta_1\eta_2. \tag{B.19}$$

The visibility is then given by

$$\mathcal{V} = \frac{\mathcal{R}_{\max.} - \mathcal{R}_{\min.}}{\mathcal{R}_{\max.} + \mathcal{R}_{\min.}} \approx \frac{[1 + \mathcal{O}] + \langle n \rangle \left(1 - \frac{1}{2}\left(\frac{\eta_1}{\eta_2} + \frac{\eta_2}{\eta_1}\right)\right)}{[3 - \mathcal{O}] + 3\langle n \rangle + \frac{1}{2}\langle n \rangle \left(\frac{\eta_1}{\eta_2} + \frac{\eta_2}{\eta_1}\right)}, \quad \text{(B.20)}$$

in the final form of which we have used the approximation that our PDC process is highly multimodal. Moreover, we see from (B.20) that if the twin beams are detected with largely different efficiencies, this causes an unbalance due to which the visibility is degraded. In our case the Klyshko efficiencies, with which signal and idler are detected, are close to each other and in good approximation we can model the measured visibilities in terms of the mean photon number as

$$\mathcal{V} \approx \frac{1 + \mathcal{O}}{3 - \mathcal{O} + 4\langle n \rangle} \quad \text{(B.21)}$$

that contains in addition to the spectral overlap known for a true photon-pair state [31] a degradation in the visibility due to the higher photon-number contributions.

References

[1] Tanzilli S, Tittel W, de Riedmatten H, Zbinden H, Baldi P, de Micheli M, Ostrowsky D B and Gisin N 2002 PPLN waveguide for quantum communication *Eur. Phys. J.* D **18** 155

[2] Fiorentino M, Spillane S M, Beausoleil R G, Roberts T D, Battle Ph and Munro M W 2007 Spontaneous parametric down-conversion in periodically poled KTP waveguides and bulk crystals *Opt. Express* **15** 7479

[3] Krapick S, Herrmann H, Quiring V, Brecht B, Suche H and Silberhorn C 2013 An efficient integrated two-color source for heralded single photons *New J. Phys.* **15** 033010

[4] Silverstone J W *et al* 2013 On-chip quantum interference between silicon photon-pair sources *Nature Photon* **8** 104

[5] Wang J *et al* 2014 Gallium arsenide (gaas) quantum photonic waveguide circuits *Opt. Comm.* **327** 49

[6] Krapick S, Stefszky M S, Jachura M, Brecht B, Avenhaus M and Silberhorn C 2014 Bright integrated photon-pair source for practical passive decoy-state quantum key distribution *Phys. Rev.* A **89** 012329

[7] Yeh P and Yariv A 1976 Bragg reflection waveguides *Opt. Comm.* **19** 427

[8] Lanco L, Ducci S, Likforman J-P, Marcadet X, van Houwelingen J A W, Zbinden H, Leo G and Berger V 2006 Semiconductor waveguide source of counterpropagating twin photons *Phys. Rev. Lett.* **97** 173901

[9] Horn R, Abolghasem P, Bijlani B J, Kang D, Helmy A S and Weihs G 2012 Monolithic source of photon pairs *Phys. Rev. Lett.* **108** 153605

[10] Bijlani B J, Abolghasem P and Helmy A S 2013 Semiconductor optical parametric generators in isotropic semiconductor diode lasers *Appl. Phys. Lett.* **103** 091103

[11] Boitier F, Orieux A, Autebert C, Lemaitre A, Galopin E, Manquest C, Sirtori C, Favero I, Leo G and Ducci S 2014 Electrically injected photon-pair source at room temperature *Phys. Rev. Lett.* **112** 183901

[12] Sarrafi P, Zhu E Y, Dolgaleva K, Holmes B M, Hutchings D C and Aitchison J S 2013 and Li Qian. Continuous-wave quasi-phase-matched waveguide correlated photon pair source on a III-V chip *Appl. Phys. Lett.* **103** 251115

[13] Caillet X, Orieux A, Lemaitre A, Filloux P, Favero I, Leo G and Ducci S 2010 Two-photon interference with a semiconductor integrated source at room temperature *Opt. Express* **18** 9967

[14] Orieux A, Eckstein A, Lemaitre A, Filloux P, Favero I, Leo G, Coudreau T, Keller A, Milman P and Ducci S 2013 Direct bell states generation on a III-V semiconductor chip at room temperature *Phys. Rev. Lett.* **110** 160502

[15] Horn R T *et al* 2013 Inherent polarization entanglement generated from a monolithic semiconductor chip *Sci. Rep.* **3** 2314

[16] Valles A, Hendrych M, Svozilik J, Machulka R, Abolghasem P, Kang D, Bijlani B J, Helmy A S and Torres J P 2013 Generation of polarization-entangled photon pairs in a Bragg reflection waveguide *Opt. Express* **21** 10841

[17] Thyagarajan K, Das R, Alibart O, de Micheli M, Ostrowsky D B and Tanzilli S 2008 Increased pump acceptance bandwidth in spontaneous parametric downconversion process using bragg reflection waveguides *Opt. Express* **16** 3577

[18] Abolghasem P, Hendrych M, Shi X, Torres J P and Helmy A S 2009 Bandwidth control of paired photons generated in monolithic bragg reflection waveguides *Opt. Lett.* **34** 2000

[19] Svozilik J, Hendrych M, Helmy A S and Torres J P 2011 Generation of paired photons in a quantum separable state in bragg reflection waveguides *Opt. Express* **19** 3115

[20] Svozilik J, Hendrych M and Torres J P 2012 Bragg reflection waveguide as a source of wavelength-multiplexed polarization-entangled photon pairs *Opt. Express* **20** 15015

[21] Kang D and Helmy A S 2012 Generation of polarization entangled photons using concurrent type-I and type-0 processes in algaas ridge waveguides *Opt. Lett.* **37** 1481

[22] Eckstein A, Boucher G, Lemaitre A, Filloux P, Favero I, Leo G, Sipe J E, Liscidini M and Ducci S 2014 High-resolution spectral characterization of two photon states via classical measurements. *Laser Photon Rev.* **8** L76

[23] Bijlani B J and Helmy A S 2009 Bragg reflection waveguide diode lasers *Opt. Lett.* **34** 3734

[24] Anderson D B and Boyd J T 1971 Wideband CO_2 laser second harmonic generation phase matched in GaAs thin-film waveguides *Appl. Phys. Lett.* **19** 266

[25] Banaszek K, U'Ren A B and Walmsley I A 2001 Generation of correlated photons in controlled spatial modes by downconversion in nonlinear waveguides *Opt. Lett.* **26** 1367

[26] Helmy A S, Abolghasem P, Stewart Aitchison J, Bijlani B J, Han J, Holmes B M, Hutchings D C, Younis U and Wagner S J 2011 Recent advances in phase matching of second-order nonlinearities in monolithic semiconductor waveguides *Laser Photon. Rev.* **5** 272

[27] Grice W P and Walmsley I A 1997 Spectral information and distinguishability in type-II down-conversion with broadband pump *Phys. Rev.* A **56** 1627

[28] U'Ren A B, Silberhorn Ch, Erdmann R, Banaszek K, Grice W P, Walmsley I A and Raymer M G 2005 Genreration of pure single photon wavepackets by conditional preparation based on spontaneous parametric downconversion *Laser Phys.* **15** 146

[29] Zhukovsky S V, Helt L G, Kang D, Abolghasem P, Helmy A S and Sipe J E 2012 Generation of maximally-polarization-entangled photons on a chip *Phys. Rev.* A **85** 013838

[30] Zhukovsky S V, Helt L G, Abolghasem P, Kang D, Sipe J E and Helmy A S 2012 Bragg reflection waveguides as integrated sources of entangled photon pairs *J. Opt. Soc. Am.* B **29** 2515
[31] Avenhaus M, Chekhova M V, Krivitsky L A, Leuchs G and Silberhorn Ch 2009 Experimental verification of high spectral entanglement for pulsed waveguided spontaneous parametric down-conversion *Phys. Rev.* A **79** 043836
[32] Brida G, Caricato V, Fedorov M V, Genovese M, Gramegna M and Kulik S P 2009 Characterization of spectral entanglement of spontaneous parametric-down conversion biphotons in femtosecond pulsed regime *Europhys. Lett.* **87** 64003
[33] Bernhard C, Bessire B, Feurer T and Stefanov A 2013 Shaping frequency-entangled qudits *Phys. Rev.* A **88** 032322
[34] Wakui K, Eto Y, Benichi H, Izumi S, Yanagida T, Ema K, Numata T, Fukuda D, Takeoka M and Sasaki M 2014 Ultrabroadband direct detection of nonclassical photon statistics at telecom wavelength *Sci. Rep.* **4** 4535
[35] Hong C K, Ou Z Y and Mandel L 1987 Measurement of subpicosecond time intervals between two photons by interference *Phys. Rev. Lett.* **59** 2044
[36] Fraine A, Minaeva O, Simon D S, Egorov R and Sergienko A V 2012 Broadband source of polarization entangled photons *Opt. Lett.* **37** 1910
[37] Zhu E Y, Tang Z, Qian L, Helt L G, Liscidini M, Sipe J E, Corbari C, Canagasabey A, Ibsen M and Kazansky P G 2013 Poled-fiber source of broadband polarization-entangled photon pairs *Opt. Lett.* **38** 4397
[38] Avenhaus M, Coldenstrodt-Ronge H B, Laiho K, Mauerer W, Wamsley I A and Silberhorn Ch 2008 Photon number statistics of multimode parametric downconversion *Phys. Rev. Lett.* **101** 053601
[39] Lumerical-Solutions-Inc. www.lumerical.com/tcad-products/mode/. 2014.
[40] West B R and Helmy A 2006 Analysis and design equations for phase matching using Bragg reflection waveguides *IEEE J. Quantum Electron* **12** 431
[41] Mizrahi A and Schächter L 2004 Bragg reflection waveguides with a matching layer *Opt. Express* **12** 3156
[42] Christ A, Laiho K, Eckstein A, Lauckner T, Mosley P J and Silberhorn C 2009 Spatial modes in waveguided parametric downconversion *Phys. Rev.* A **80** 033829
[43] Abolghasem P, Han J, Bijlani B J and Helmy A S 2010 Type-0 second order nonlinear interaction in monolithic waveguides of isotropic semiconductors *Opt. Express* **18** 12681
[44] Zhong T, Wong F N C, Roberts T D and Battle P 2009 High performance photon-pair source based on a fiber-coupled periodically poled $KTiOPO_4$ waveguide *Opt. Express* **17** 12019
[45] Harder G, Ansari V, Brecht B, Dirmeier T, Marquardt C and Silberhorn C 2013 An optimized photon pair source for quantum circuits *Opt. Express* **21** 13975
[46] Eckstein A, Christ A, Mosley P J and Silberhorn C 2011 Highly efficient single-pass source of pulsed single-mode twin beams of light *Phys. Rev. Lett.* **106** 013603
[47] Klyshko D N 1977 Utilization of vacuum fluctuations as an optical brightness standard *Sov. J. Quantum Electron* **7** 591
[48] Christ A, Laiho K, Eckstein A, Cassemiro K N and Silberhorn C 2011 Probing multimode squeezing with correlation functions *New. J. Phys.* **13** 033027
[49] Keller T E and Rubin M H 1997 Theory of two-photon entanglement for spontaneous parametric down-conversion driven by a narrow pump pulse *Phys. Rev.* A **56** 1534
[50] Grice W P, U'Ren A B and Walmsley I A 2001 Eliminating frequency and space-time correlations in multiphoton states *Phys. Rev.* A **64** 063815
[51] Schlawin F and Mukamel S 2013 Photon statistics of intense entangled photon pulses *J. Phys. B: At. Mol. Opt. Phys.* **46** 175502